Int. J. Electrochem. Sci., 14 **(2019)** 8819 – 8835, doi: 10.20964/2019.09.26

International Journal of
ELECTROCHEMICAL
SCIENCE
www.electrochemsci.org

Aminoethanesulfonic Acid- Based Blends for Inhibition of J55 Steel Corrosion in Simulated Oilfield Pickling Fluid

Xianming Liu[1,2], Jiajia Jing[3,], Qiang Fu[4], Qiong Li[1], Su Li[5], Yaguang Qu[6], Ambrish Singh[7]*

[1] School of Mechanical Engineering, Yangtze University, Jingzhou,434000, China.
[2] Drilling & Production Technology Research Institute, CCDE, CNPC, Guanghan 618000, China
[3] Safety, Environment, Quality Supervision & Testing Research Institute, CCDE, CNPC, Guanghan 618000, China.
[4] PetroChina Southwest Oil & Gasfield Company Engineering Technology Research Institute, Chengdu, 610000, China.
[5] Shunbei oil and gas management department, SINOPEC Xibei branch company, Urumchi, 830001, China.
[6] School of Petroleum Engineering, Yangtze University, Wuhan, 430100, China.
[7] School of Materials Science and Engineering, Southwest Petroleum University, Chengdu, China.
[*]E-mail: jingjiajia88@163.com

Received: 25 March 2019 / *Accepted:* 19 May 2019 / *Published:* 31 July 2019

As industries are more interested in patronizing non-toxic and ecofriendly inhibitors to preserve environment, two binary and a ternary blend have been formulated from 2-aminoethanesulphonic acid (2ASA) and some synergistic intensifiers. The blends have been demonstrated as efficient corrosion inhibitors in simulated pickling fluid for protection of J55 steel materials used in oilfield. Small concentration (10^{-3} M) of the base compound, 2ASA, was 96.4% efficient at 30 ^{o}C but far less efficient at high temperature (90 ^{o}C). Due to synergistic effects of the compounds used to formulate the blends, it was possible to record efficiency up to 87.8% at 90 ^{o}C for one of the blends containing potassium iodide (KI) and dipotassium hydrogen phosphate (DPHP). Adsorption of 2ASA molecules was spontaneous, exothermic and involves monolayer of physisorbed molecules on J55 steel surface as best approximated by Langmuir adsorption model. Tafel measurements confirm that 2ASA behaves as mixed type inhibitor with domino inhibitive influence on anodic half reaction. FTIR and EDAX studies confirm that adsorption of 2ASA is facilitated by N, S, and O functionalities. Formation of surface adsorbed 2ASA film was visibly observed via scanning electron microscopy (SEM). Inhibition efficiencies of 2ASA were determined by weight loss, electrochemical impedance spectroscopy (EIS) and potentiodynamic polarization (PDP) techniques and results were consistent and comparable. 2ASA and its blends could find application as alternative ecofriendly corrosion inhibitors for pickling and similar acidizing operations in the oilfield.

Keywords: 2-aminoethanesulphonic acid, pickling corrosion inhibitor, adsorption, inhibitor blends, SEM/EDS, EIS.

1. INTRODUCTION

Injection of acid into oil and gas formation is a recovery enhancement procedure aimed at either to pickle or clean the wellbore of scales and mineral deposits or to stimulating the well, dissolve formation rock to free trapped hydrocarbons and etching to open new flow channels. For this procedure, commonly referred to as acidizing, hydrochloric acid (HCl) is often used. Compared to other acids associated with oilfield acidizing job, HCl is relatively more cost effective and of low toxicity. When deployed for pickling and washing of scales from pipework, it dissolves many inorganic scales and debris completely because many of them are soluble in HCl. When used for treatment of reservoir formation, the rate of dissolution of carbonate rocks by HCl is fast and complete reaction is achievable compared to other acids such as hydrofluoric and acetic acids. However, the adverse effect of using HCl is that it is very corrosive, hence it corrodes steel materials which it contacts during the process. In other words, while acidizing improves recovery, it creates the problem of corrosion which is expensive to manage and has resulted in increased production cost globally.

Since continuing production using well acidizing intervention technique is more economical than abandoning the well to drill new ones, the acid is usually mixed with small concentrations of corrosion inhibitors to slow down the rate of corrosion. Corrosion inhibitors do not stop corrosion, and should not react with the acid, in order to sustain the acid in the live state for the pickling or acidizing jobs. Bearing these in mind, and other factors such as the cost of the inhibitor, its ready availability and impact on environment in terms of toxicity, various corrosion inhibitors have been designed from organic compounds [1-5] and extracts/isolates from plant materials [6-10] for various alloys. A feature usually considered when selecting an organic compound to be tested as corrosion inhibitor is the presence of some functionalities such as heteroatoms (O, N, S, and P), aromatic or heterocyclic rings and multiple bonds in its molecular structure [11, 12]. For plant materials, there are several classes phytocompounds including alkaloids, steroids, tannins, flavonoids, anthraquinones, terpenoids and polyphenols [13, 14] which are already rich in the functionalities listed above.

The corrosion inhibitor acts by adsorption through its active sites on the active site on the alloy surface [15]. In the case of steel, which is mainly composed of iron, the interaction between the inhibitor species and the iron ions can be driven physical or chemical forces. It is necessary that the interactive force be strong enough to keep the inhibitor active at severely corrosive environments. For instance, in the oilfield, as the injected acid travels down the hole, increase in temperature increases the acid corrosion rate thus creating more sever corrosive environment. Many reported corrosion inhibitors are tested at room temperature [16] and some others not above 60 ^{o}C [17]. Thus, their efficiency at downhole conditions is not known. In this study, we investigated 2ASA as an alternative corrosion inhibitor for acidizing jobs such as acid wash and pickling which involves low concentration HCl. We have checked its performance at downhole conditions by simulating higher temperature environments up to 90 ^{o}C in the laboratory in aqueous phase.

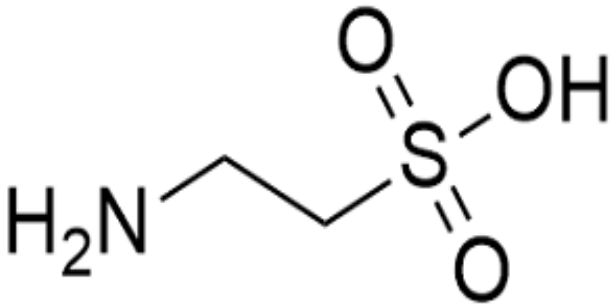

Figure 1. Structure of 2ASA showing potential adsorption sites.

2ASA is a bio-based material which contains most of the functional groups listed earlier associated with efficient corrosion inhibitors. The molecular structure of 2ASA is shown in Fig. 1. It is non-toxic and can be cheaply obtained from biological and human sources [18-20]. Its efficiency was tested at different temperatures using weight loss and electrochemical techniques. Surface characterization techniques were also used to study the extent of protection and mode of its interaction with the steel surface. The choice of J55 steel was motivated by its frequent use for construction of pipework and well structural materials in the oil and gas industry due to its corrosion resistant properties [21, 22]. 2ASA was also blended with some synergistic compounds, namely, potassium iodide (KI) and dipotassium hydrogen phosphate (DPHP) which are known compounds that act in synergy with organic corrosion inhibitors to intensify their efficiencies [23]. A commercial inhibitor is also tested under the same conditions to compare the efficiency with the new blends investigated. This study documents the efficiency of blends of 2ASA and synergistic compounds in laboratory simulated pickling solution at temperatures up to 90 ^{o}C in comparison with a commercially obtained corrosion inhibitor.

2. MATERIALS AND METHODS

2.1 Metal specimens and surface preparation

Depending on the experiment used, different dimensions of J55 steel coupons supplied by Qingdao Tengxiang Instrument and Equipment Co. Ltd., China and the chemical composition was C (0.065), Si (0.24), Mn (1.58), P (0.011), S (0.003), Cu (0.01), Cr (0.022), Nb (0.057), V (0.005), Ti (0.024), B (0.0006), Fe (balance). The coupons for gravimetric experiments were of dimension 2 cm x 2 cm x 0.5 cm, for electrochemical measurements was 1 cm × 1 cm x 0.5 cm and for surface analysis examination was 2 cm × 1 cm x 0.5 cm. ASTM procedures were followed to prepare the steel surfaces [24] and in addition, the coupons for electrochemical measurements were finish to mirror surface using CC-22F P2000 grade.

2.2 Test solutions

1 M HCl, prepared by diluting Analytical grade 37% HCl with distilled water according to dilution principle, was used as simulated pickling fluid. Industrial grade 2ASA supplied by Meyers Co. Ltd., China was prepared (as received, with no further characterization/purification) in the acid solution in the concentrations range of 1×10^{-4} to 10×10^{-4} M. The other synergistic compounds (KI and DPHP) were prepared to concentration of 1 x 10^{-4} M and blended with 2ASA in the ration 1:1.

2.3 Gravimetric measurements

Coupons were pre-weighed, immersed in the respective test solutions and their containers (covered) were placed in water bath maintained at 30 ºC. After 5 h, they were retrieved and cleaned using ASTM G31 standard procedures, dried in air after rinsing in acetone [24]. Triplicates of the same experiment was conducted per test solution and repeated for other temperatures (50, 70 and 90 ºC). The weight losses were used to calculate the average corrosion rate (CR) of iron given that its density is ρ (gcm^{-3}), average surface area is A (cm^2) and immersion time is t (h) according to Eq. 1 [23]. The corrosion inhibition efficiency (E_W, %) and degree of surface coverage (θ) were calculated using Eq. 2 and 3 respectively.

$$CR = \frac{87.6(m_o - m_1)}{\rho A t} \quad (1)$$

$$E_W = 100\left(\frac{CR_a - CR_i}{CR_a}\right) \quad (2)$$

$$\theta = 0.01E_W \quad (3)$$

where m_o and m_1 are the weights of the coupons before and after immersion in the test solutions, CR_a and CR_i are the corrosion rates of steel in the acid and inhibited solutions.

2.4 Electrochemical monitoring

Electrochemical measurements were conducted using the Gamry ZRA (REF 600-18042) electrochemical workstation consisting of the conventional three electrodes set up (saturated calomel electrode (SCE) as reference electrode, platinium as counter electrode and J55 steel coupon as working electrode). Before the actual experiments, the steel electrode was left in the solution for 30 minutes to encourage corrosion to occur so that open circuit potential (OCP) can stabilize [25]. Impedance measurements (EIS) were conducted at frequency of 10^5 to 10^{-2} Hz at 30 ºC. Voltage of -0.15 V to +0.15 V *vs.* OCP at 0.2 mV/s scan rate was set for potentiodynamic polarization measurements [25]. Gamry E-Chem software package was used for data fitting and analyses. Charge transfer resistance and corrosion current densities were used to calculate the inhibition efficiencies for EIS (E_E) and PDP (E_P) measurements according to Eq. 4 and Eq. 5 respectively [25].

$$E_E = 100\left(\frac{R_{ctI} - R_{ctB}}{R_{ctI}}\right) \quad (4)$$

$$E_P = 100\left(1 - \frac{I^i_{corr}}{I^b_{corr}}\right) \quad (5)$$

where R_{ctB} and R_{ctI} are measured charge transfer resistances without and with inhibitor respectively, and I^{b}_{corr} and I^{i}_{corr} are the measured corrosion current densities without and with inhibitor respectively. The magnitude of the double layer capacitance (C_{dl}) of the adsorbed film was calculated from constant phase element (CPE) constant (Y_o) and charge transfer resistance (R_{ct}) using Eq. 6 [25].

$$C_{dl} = (Y_0 \, {R_{ct}}^{n-1})^{\frac{1}{n}} \quad (6)$$

where *n* is a constant obtained from the phase angle given that $(j^2 = -1)\alpha$ and $n = 2\alpha/\pi$).

2.6 FTIR spectroscopy

Concentration of 2ASA used was 10 x 10^{-4} M ASA in 1 M HCl solution. The spectrum of the pure 2ASA sample (as supplied) and that of the film formed on J55 steel surface after 5 h immersion (both mixed with potassium bromide) were recorded.

2.7 SEM-EDAX study

Steel coupons polished as described above were used for this experiment. The SEM images were recorded in the vacuum mode before and after immersion in 1 M HCl for 5 h. This was repeated with a coupon immersed in HCl containing 10x10^{-4} M 2ASA solution. The instrument was operated at 5 kV. EDAX profiles of the J55 steel surfaces were equally also recorded.

3. RESULTS AND DISCUSSION

3.1 Corrosion inhibition by 2ASA

Corrosion of J55 steel in the immersed solutions resulted in loss of its weight. The corrosion rate in 1 M HCl was 39.51 mmpy at 30 ^{o}C. When 2ASA was added, the corrosion rate decreased as can be observed in Table 1. The corrosion rate was as low as 1.42 mmpy at 10 × 10^{-4} M. With the inhibitor, corrosion rate decreased with increase in concentration, which implies increase in inhibitive effect of 2ASA as its concentration increases. The highest concentration of 2ASA was 96.4 % efficient at 30 ^{o}C and compared closely with the commercial inhibitor tested in the control experiment at that temperature.

3.2 Effect of temperature on inhibition efficiency

For acidizing procedure, the corrosivity of the acid often increases as it moves downhole due to increase in temperature. The efficiency of 2ASA at increased temperature was investigated by increasing the temperature progressively to 50, 70 and 90 ^{o}C. It was observed that J55 steel corrodes at higher rate as temperature increases. The corrosion rate in 1 M HCl was 308.63 mmpy at 90 ^{o}C but reduced to 53.63 mmpy in the presence of 10 × 10^{-4} M 2ASA. The inhibition efficiency of 10 × 10^{-4} M 2ASA decreased

from 96.4% at 30 ºC to 82.6% at 90 ºC perhaps due to its thermal degradation. The lower concentrations of 2ASA were less efficient as can be seen in the values displayed in Table 1.

Table 1. Corrosion rate of J55 steel and inhibition efficiency of 2ASA inhibited 1 M HCl solution at 30 – 90 ºC.

2ASA Concentration (10^{-4}M)	**30 ºC**		**50 ºC**		**70 ºC**		**90 ºC**	
	CR **(mmpy)**	E_W **(%)**	***CR*** **(mmpy)**	E_W **(%)**	***CR*** **(mmpy)**	E_W **(%)**	***CR*** **(mmpy)**	E_W **(%)**
0	39.5	-	98.6	-	182.9	-	308.2	-
1	9.7	88.1	16.4	83.4	51.6	71.8	112.5	63.5
2	3.8	90.3	13.1	86.7	42.1	77.0	91.2	68.8
5	2.1	94.7	11.8	88.0	36.2	80.2	81.1	73.7
10	1.4	96.4	8.7	91.2	21.4	88.3	53.6	82.6

3.3 Effects of synergistic compounds

It has been reported that PI, MC and CC can synergistically increase the efficiency of many organic corrosion inhibitors [23]. Based on this, 10×10^{-4} M 2ASA was blended with each of KI and DPHP in the ratio 1:1 to improve the inhibition efficiency especially at high temperatures. The binary blends were also tested under the same conditions with a commercial inhibitor (COM-INH) for comparison. The results (Table 2) show that all the blends were more efficient than 2ASA alone at all temperatures. Therefore, the compounds added all acted synergistically with 2ASA and the highest synergism was observed with KI. Improvement of efficiency of 2ASA by DPHP was better than KI at all temperatures. The ternary blend containing 2ASA, KI and DPHP in the ration 1:1:1 was more efficient especially at 90 ºC and compared closely with the commercial inhibitor especially below 70ºC.

Table 2. Inhibition efficiency of 2ASA blended with some synergistic compounds.

Formulation Composition	**Inhibition efficiency at different temperatures**			
	30 ºC	**50 ºC**	**70 ºC**	**90 ºC**
2ASA	99.4	94.0	89.6	82.6
2ASA+KI	99.8	98.0	92.4	84.1
2ASA+DHDP	99.8	98.4	92.7	85.6
2ASA+DHDP+KI	99.9	99.2	93.8	87.8
COM- INH	100.0	100.0	99.9	99.8

3.4 Corrosion inhibitor adsorption

The nature of adsorptive interactions between corrosion inhibitor molecules and the surface they protect is often predicted by plotting the surface coverage data as a function of concentration as provided by various adsorption isotherm models [26]. The fractional surface coverage values obtained in this

study were fitted into Temkin, Langmuir, Freundlich and El-Awady et al adsorption isotherms [27-29]. The highest values of R^2 were obtained with Langmuir adsorption isotherm (Fig. 2) on linearizing the plots, hence the adsorption of 2ASA was explained based on this model. For adsorbate of concentration (C) condensing (adsorption) on and evaporating from (desorption) a surface with a fractional coverage (θ), if K_{ads} is the equilibrium constant relating the adsorption-desorption terms, the Langmuir equation for the adsorption is given in Eq. 7 [30]. The free energy of adsorption (ΔG_{ads}) can be determined in terms of K_{ads} using Eq. 8 [28].

$$\frac{C}{\theta} = C + \frac{1}{K_{ads}} \quad (7)$$

$$\Delta G_{ads} = -RT \ln(55.5 K_{ads}) \quad (8)$$

where R is the universal gas constant, T is the absolute temperature and 55.5 is the concentration of water. Adsorption parameters were calculated and are displayed in Table 3.

Table 3. Some parameters for the adsorption of 2ASA on J55 steel surface immersed in 1 M HCl solution.

Parameters	30 ºC	50 ºC	70 ºC	90 ºC
Slope	0.98	1.1	1.2	1.3
K_{ads} (M^{-1})	7.8	2.7	1.1	0.7
ΔG_{ads} ($kJmol^{-1}$)	-14.1	-13.5	-11.8	-10.4

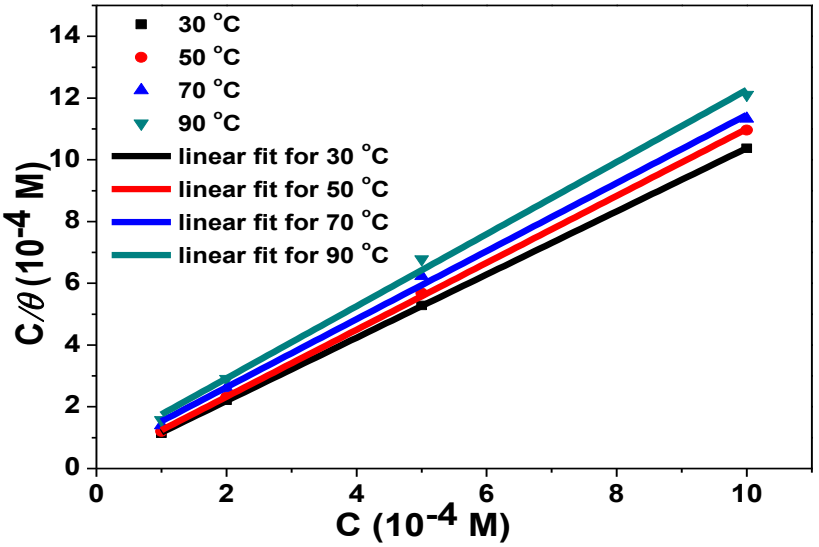

Figure 2. Langmuir adsorption isotherm for the inhibition of J55 steel corrosion in 1 M HCl using different concentrations of 2ASA at 30 – 90 ºC.

The slopes of the plots are very close to unity indicating that the adsorption of 2ASA follows the Langmuir model closely and that a monolayer of 2ASA molecules is formed. The slight differences in K_{ads} from unity values at different temperatures indicate that there are slight interactions between 2ASA molecules and J55 steel surface. The strength of adsorptive binding of 2ASA to J55 steel evidenced in K_{ads} values is seen to decrease as temperature increases. This trend suggests that the adsorption

mechanism is physical in nature and is also confirmed by the values of ΔG_{ads} which are less negative than -20 kJmol^{-1} at all temperatures [26]. The adsorption is also spontaneous at all temperatures as evidenced in the negative values of ΔG_{ads}. These imply that the 2ASA molecules diffuse from the bulk fluid towards the steel surface on their own without any external influence. On reaching the proximities of the surface, they interact with surface molecules and form adsorbed protective film held to the surface via electrostatic or van der Waals forces. As temperature increases, the binding strength weakens and maybe desorption of some 2ASA occurs [31].

3.5 Kinetic and thermodynamic study

The logarithms of corrosion rate values were plotted against the reciprocals of absolute temperatures (Fig. 3) according to the linear form of Arrhenius equation shown in Eq. 9. The values of slope and intercept were used to calculate the activation energy and frequency factor for each test solution.

$$\log CR = \log A - \frac{E_a}{2.303RT} \quad (9)$$

where A is the Arrhenius pre-exponential or frequency factor and E_a is the activation energy.

It was found out that the magnitude of E_a for 1 M HCl was lower than the its inhibited counterparts (Table 4). It has been reported that when the activation energy of the inhibited solution is greater than that of the uninhibited solution, as obtained in this study, the adsorption of the inhibitor follows physisorption mechanism [26]. This is in agreement with the prediction made from adsorption study and confirms physical adsorption mechanism.

The corrosion rate values were also fitted into the classical thermodynamic equation (Eq. 10). Transition state plots of $\log(\frac{CR}{T})$ against inverse of temperature (1000/T) were constructed as shown in Fig. 4. Some thermodynamic parameters such as heat change (ΔH^*) and entropy change (ΔS^*) for the activation process were also calculated from the slope and intercept of the plots respectively and are also presented in Table 4.

$$\log(\frac{CR}{T}) = \left[\left(\log\left(\frac{R}{Nh}\right) + \left(\frac{\Delta S^*}{2.303R}\right)\right)\right] - \left(\frac{\Delta H^*}{2.303RT}\right) \quad (10)$$

The ΔH^* values are all negative which point to the exothermic nature of the adsorption process at all temperatures. In some published works, it is opined that when ΔH^* value is less than zero, physical adsorption occurs [32].

Table 4. Activation parameters for the inhibition of J55 steel corrosion in 1 M HCl containing different concentrations of 2ASA at 30 - 90 ^{o}C.

2ASA Conc (x 10^{-4} M)	E_a **(kJmol^{-1})**	A	ΔH^* **(kJmol^{-1})**	ΔS^* **(kJmol^{-1})**
0	38.2	7.9 x 10^6	-28.1	0.3
1	48.7	3.3 x 10^7	-35.6	0.3
2	53.3	9.8 x 10^7	-45.9	0.2
5	55.7	8.5 x 10^8	-51.2	0.2
10	64.3	3.1 x 10^{10}	-52.5	0.2

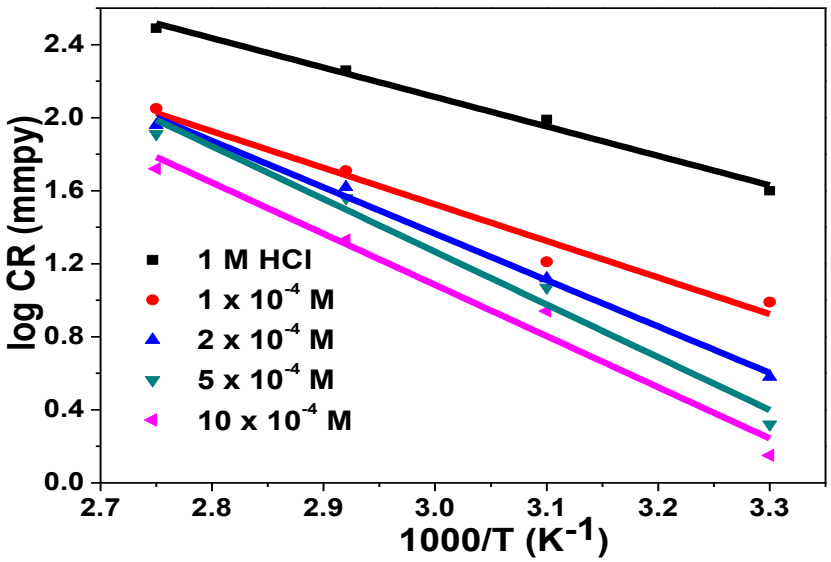

Figure 3. Arrhenius plot for the corrosion of J55 steel in 1 M HCl without and with different concentrations of 2ASA at 30 – 90 ºC.

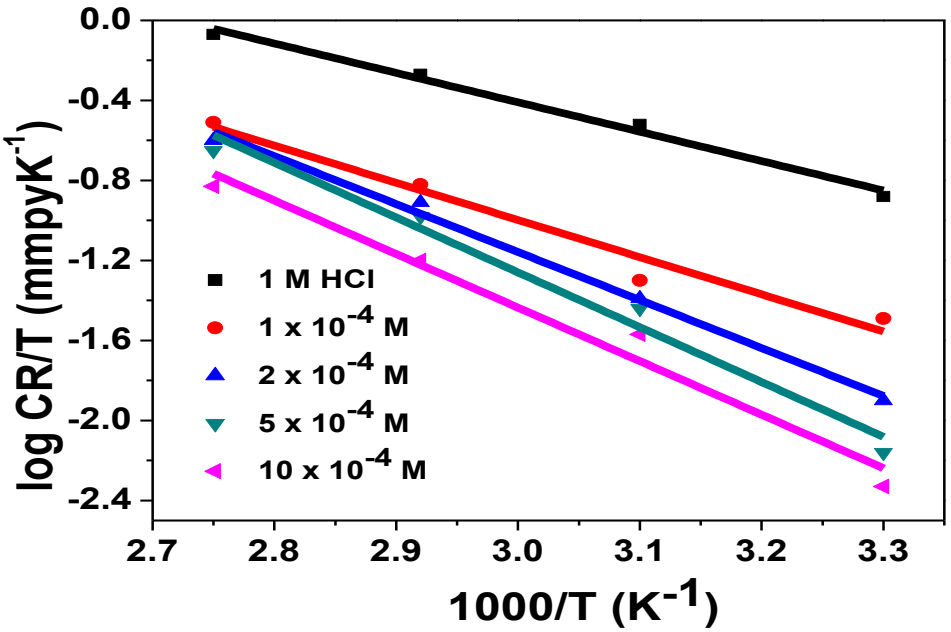

Figure 4. Transition state plot for the corrosion of J55 steel in 1 M HCl without and with different concentrations of 2ASA at 30 – 90 ºC.

Some authors also suggest that it is physisorption when ΔH^* values are less negative than -40 kJmol^{-1}; chemisorption if more negative than -100 kJmol^{-1}; and a combination of both mechanisms if in-between both limits [26]. The range of ΔH^* values obtained strongly supports physisorption mechanism with slight possibility of simultaneous physisorption and chemisorption at concentrations above 2 x 10^{-4} M. Also, the values of ΔS^* reduce as concentration increases, implying that adsorption of more 2ASA molecules results in decrease in entropy of the entire (bulk) solution.

3.6 Electrochemical measurements

As an alloy, J55 steel contains mainly iron and some other metals earlier stated.Different reactions could take place at the anode; a typical scheme is shown in Eq. 11. The oxidation reaction of Fe in the steel is depicted in Eq. 12. The cathodic reaction involves reduction of water followed by evolution of hydrogen (Eq. 13 -14) [33, 34].

Anodic reaction:

$$M_{(s)} \rightarrow M^{n+} + ne^{-} \quad (11)$$

$$Fe_{(s)} \rightarrow Fe^{2+}_{(aq)} + 2e^{-} \quad (12)$$

Cathodic reaction:

$$2H^{+}_{(aq)} + 2e^{-} \rightarrow H_{2(g)} \quad (13)$$

$$H_2O + 2e^{-} \rightarrow H^{+} + OH \quad (14)$$

With potentiodynamic polarization measurement, control over the potential, which is the driving force, can be achieved, so as to quantify the current based in net change in reaction rate. The corrosion current density (I_{corr}), which is a kind of compromise current, and the corresponding compromise potential (E_{corr}) were determined after rationalizing the anodic and cathodic branches of the Tafel plots (Fig. 5). The Tafel cathodic (β_c) and anodic constants (β_a) alongside other associated parameters were also gotten and displayed in Table 5.

Table 5. PDP parameters for J55 steel corrosion in 1 M HCl without and with different concentrations of 2ASA.

Parameters	**1 M HCl**	**1 x 10^{-4} M**	**2 x 10^{-4} M**	**5 x 10^{-4} M**	**10 x 10^{-4} M**
β_a (mV/decade)	113	95	93	99	91
β_c (mV/decade)	88	86	87	88	90
I_{corr} (μA)	818	147	113	83	64
E_{corr} (V)	-0.472	-0.471	-0.467	-0.465	-0.463
$\mathcal{E}_{PDP}$ (%)	-	82	86	90	92

The value of I_{corr} obtained was found to decrease with increasing 2ASA concentration. The highest value of I_{corr} was obtained in uninhibited 1 M HCl solution. This may be as a result of formation of adsorbed thin film of 2ASA on the steel surface. The values of E_{corr} also obtained in the uninhibited acid was found to be more negative compared to values obtained from the inhibited solutions. Thus, there was a displacement of E_{corr} towards more positive values. This behavior is usually characteristic of the anodic class of corrosion inhibitors [35]. This anodic class of corrosion inhibitors often show dominant influence on the partial anodic reaction. The influence on anodic reaction is associated with slowing down of oxidation/corrosion rate of the steel through loss of electrons. However, to be sufficient for categorizing as anodic or cathodic inhibitor, the displacement in E_{corr} needs to be up to a maximum of -85 mV for the inhibited solution when compared to the uninhibited corrodent [36]. Since the displacement obtained for 2ASA was not up to this benchmark, 2ASA can be viewed to act as mixed type inhibitors but with anodic predominance. Acting that way, the compound has inhibiting influence

on both inhibits both the iron dissolution (anodic) reaction and hydrogen production (cathodic) half reaction, but with greater influence on inhibiting iron oxidation. This often occurs by mechanism of inhibition which may be controlled by activation or diffusion.

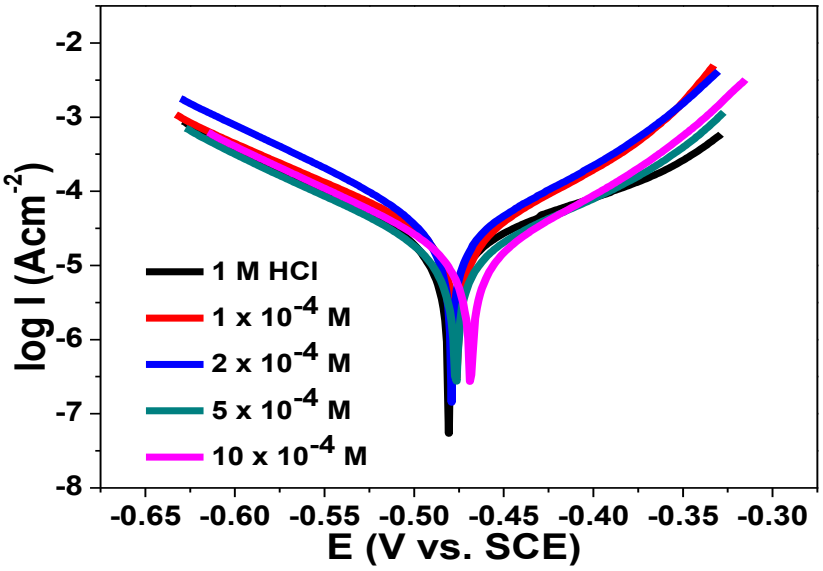

Figure 5. Potentiodynamic polarization curves for J55 steel corrosion in I M HCl without and with different concentrations of 2ASA.

EIS data obtained were directly used in constructing the Nyquist plots shown in Fig. 6. The shapes of the plots were imperfect depressed semicircles and this shape was same without and with inhibitor, showing that corrosion mechanism is the same in all the test solutions. The size of diameters of the plots increased proportionately with the concentration of the ASA which shows that concentration has effect on the corrosion inhibition efficiency. The observed imperfection. It can also be inferred from the shape of the graph that the surface of electrode (though polished) were either rough or inhomogeneity of the steel surface [37, 38]. The appearance of a single capacitive loop indicates that the corrosion mechanism is controlled by charge transfer process.

The R_s $(R_{ct}\emptyset_{CPE})$ equivalent circuit (Fig.7) model was used to fit the experimental data and good fitness (in orders of 10^{-4}) was obtained, indicating good correlation with the model used. The constant phase element (CPE) is used to compensate surface roughness or inhomogeneity of the steel [39]. The CPE can be estimated using Y_0 and n, related to impedance by Eq. 15:

$$Z_{CPE} = = (Y_0)^{-1}(jw)^{-n} \quad (15)$$

where Z_{CPE} is the impedance of the CPE, Y_0 is the CPE constant, w is the angular frequency. Some EIS parameters calculated are presented in Table 6.

The values of n increases when the inhibitor concentration increases, perhaps due to surface roughness of the steel is increased by adsorption of 2ASA [40]. The CPE could be considered as not being a pure or single resistance, capacitance or inductive element, but a relative and/or integrated influence of all these. Adsorption of more inhibitor molecules as its concentration increases results in decrease in double layer capacitance, and shows increase in dielectric nature within the electrode-water

interface. The Bode modulus and phase angle plots (Fig. 8) show distinct regions corresponding capacitance and charge transfer resistance. A close look at the trend of inhibition efficiency values reveals a consistent measurement and well as comparable values as obtained with PDP measurements.

Table 6. EIS parameters for J55 steel corrosion in 1 M HCl without and with different concentrations of 2ASA.

EIS Parameters	1 M HCl	1 x 10^{-4} M	2 x 10^{-4} M	5 x 10^{-4} M	10 x 10^{-4} M
R_{ct} (Ωcm^2)	128.6	781.4	1099.2	1581.3	1672.8
R_s (Ωcm^2)	1.022	1.116	1.137	1.211	1.227
$Y_o x10^{-6}$ ($\Omega^{-1}s^n cm^{-1}$)	162.8	144.0	153.3	142.5	144.8
n	0.825	0.831	0.840	0.859	0.878
C_{dl} x10^{-9} (F)	141.7	77.8	55.1	30.3	12.7
ε_{wl} (%)	-	83.5	88.3	91.8	92.3

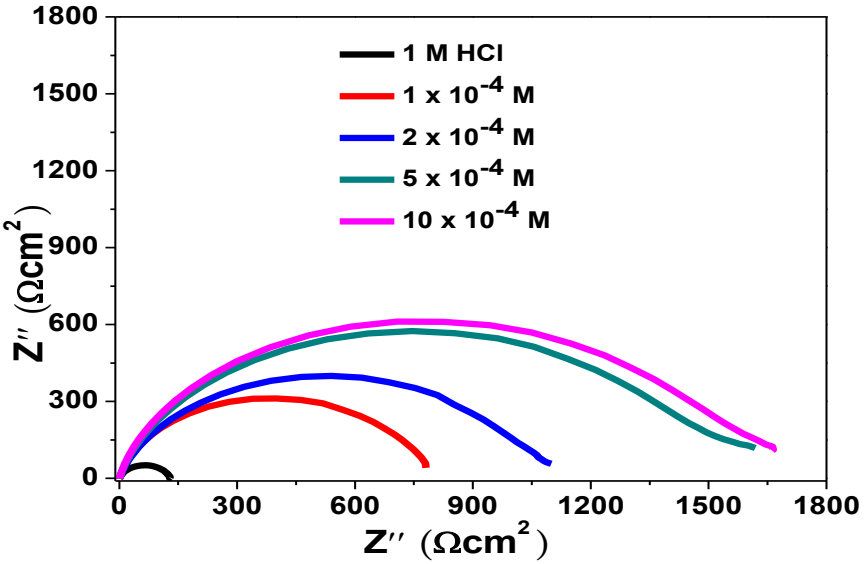

Figure 6. Nyquist plots for J55 steel corrosion in I M HCl without and with different concentrations of 2ASA.

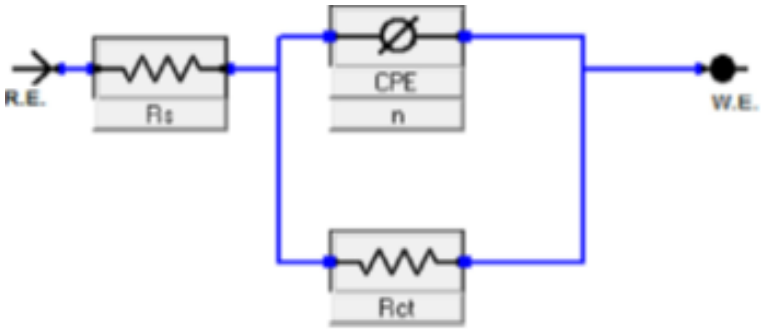

Figure 7. Equivalent circuit used for EIS data analyses

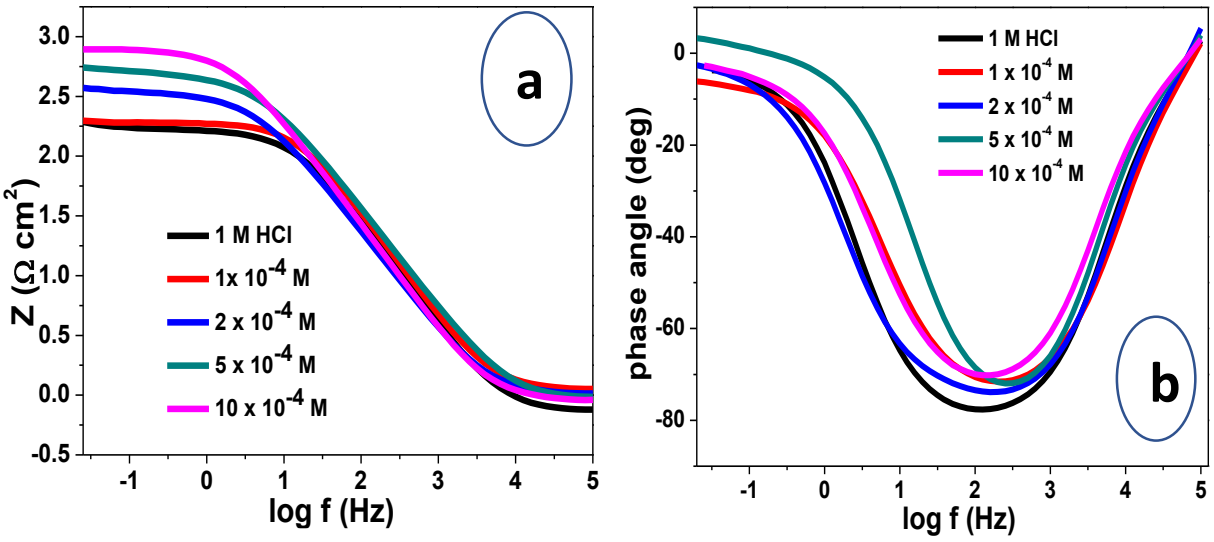

Figure 8. (a) Bode modulus and (b) phase angle plots for J55 steel corrosion in I M HCl without and with different concentrations of 2ASA.

3.7 FTIR studies

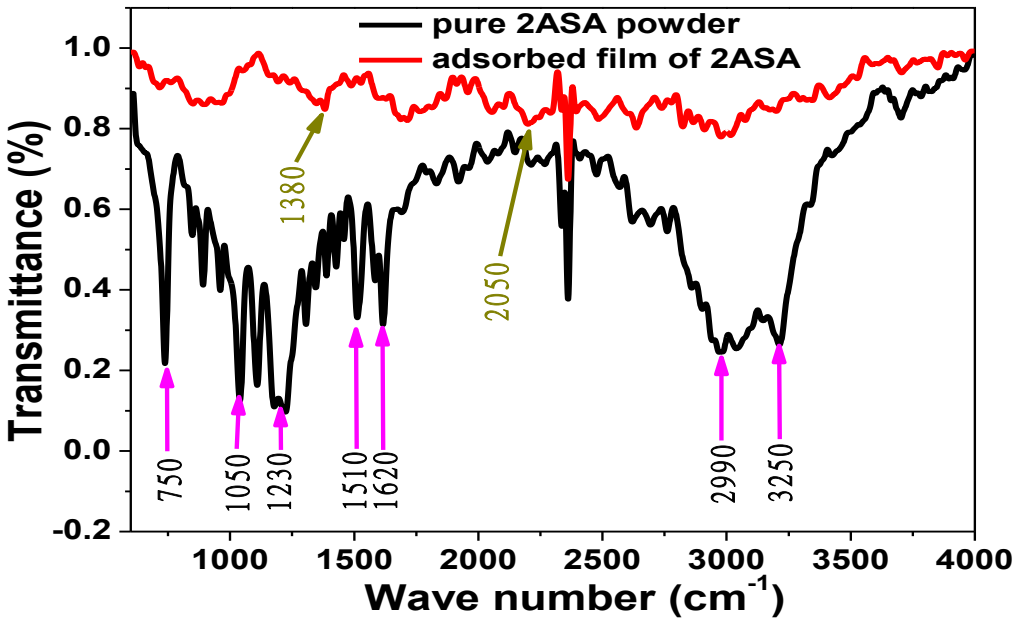

Figure 9. FTIR spectral profile of pure 2ASA and adsorbed film of 2ASA after immersion of J55 steel.

The spectrum of powder 2ASA shows some distinct peaks as shown in Fig. 9. Based on pre-knowledge of the molecular structure of 2ASA and some published data on the infrared spectrum same molecule [41-43], it is easy to assign some peaks to the major functional groups. For instance, the peaks around 1050 cm^{-1} and 1230 cm^{-1} is assigned to SO_2 stretching or bending vibrations. C-C-N stretch can also result in the peak between 1050 cm^{-1} and 1230 cm^{-1}. These peaks are not present in the spectrum of

the adsorbed film, which indicates that they may have been involved in the adsorption process. It is also possible that their participation in the adsorbed film may have caused their modification to the new peak found around 1380 cm^{-1} in the spectrum of the adsorbed film. Also, the prominent peaks at 1510 cm^{-1} and 1620 cm^{-1} are assigned to asymmetric -NH_2 bending vibrations while the one at 3250 cm^{-1} is assigned to -O-H or -NH_2 vibrations. These peaks are less prominent in the spectrum of the surface film. It can therefore be inferred from this results that the sites involved in the adsorption of 2ASA on J55 steel are N, S, and O present in the 2ASA structure.

3.8 SEM/EDS characterization

To observe the extent of protection of the steel surface by 2ASA, the morphology of J55 steel surface immersed in 1 M HCl without and with $10x10^{-4}$ M 2ASA was checked using SEM [44]. Without 2ASA, the steel experienced great corrosive damage with several pits in the acid solution as shown in Fig. 10 (a). However, in the presence of 2ASA, the surface is not as damaged as seen in Fig. 10 (b). This supports that 2ASA forms a protective film (somehow visible in the image) and inhibits the corrosion of the steel in the acid solution.

The elemental composition of the steel surface was also checked by EDS in 1 M HCl without and with 2ASA and results show differences in the amounts of N, S and O. EDS profiles before and after corrosion inhibition is shown in Fig 11 while the amounts of elements found on the steel surface is given in Table 7. It was observed that without 2ASA, the surface was composed of mainly Fe, C and O. But on addition of 2ASA, the amount of Fe decreased while the percentages of C and O increased and S and N were seen in addition. It can be stated from this that the adsorption involves these sites, hence EDS results agrees with FTIR results.

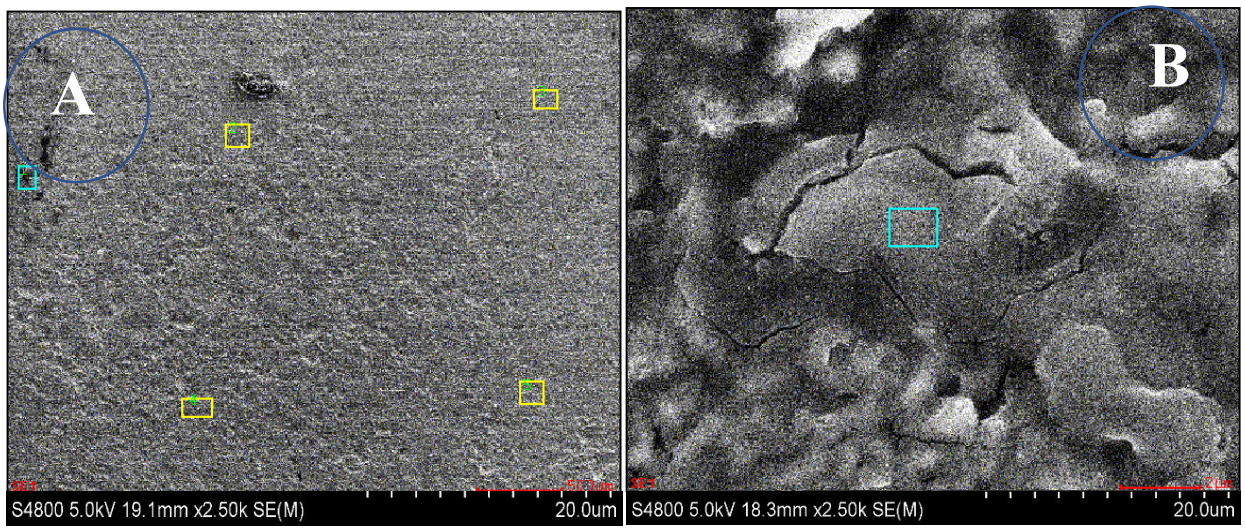

Figure 10. SEM micrographs of J55 steel surface in (a) 1 M HCl and (b) 1 M HCl containing 2ASA.

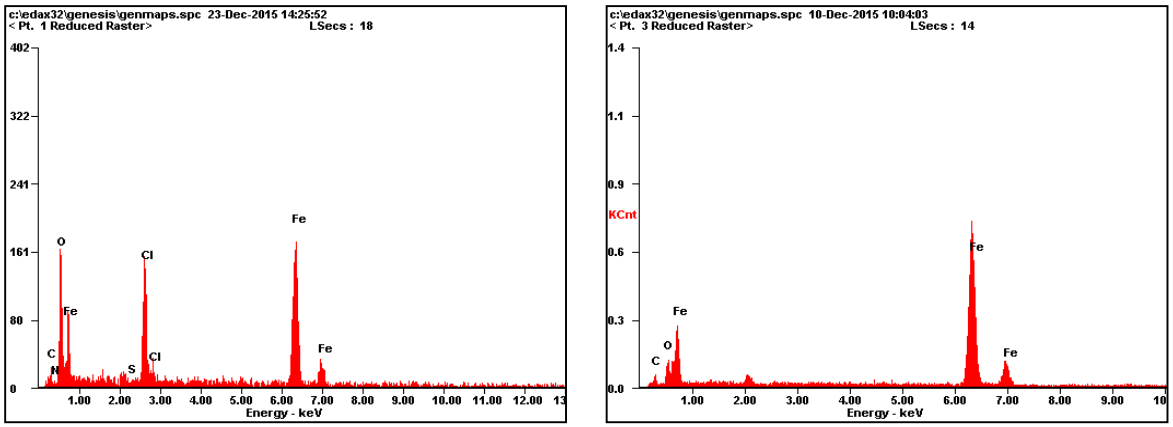

Figure 11. EDS profiles of J55 steel surface in 1 M HCl (left) and 1 M HCl containing 2ASA (right).

Table 7. Elemental composition of J55 steel surface immersed in 1 M HCl without and with 2ASA determined by EDS.

Element	**Absence of GLT**		**Presence of GLT**	
	Wt %	**At %**	**Wt %**	**At %**
C	14.78	32.36	15.03	35.03
O	09.16	19.08	11.92	20.64
N	-	-	01.30	03.86
S	-	-	01.42	02.75
Fe	76.14	48.56	70.33	37.72

4. CONCLUSIONS

2-aminoethanesulphonic acid (2ASA) and three blends prepared from it were investigated as corrosion inhibitor for J55 steel in simulated oilfield pickling fluid. All the inhibitor blends were more efficient at high temperatures up to 90 ^{o}C except 2ASA single inhibitor system. Potassium iodide and dipotassium hydrogen phosphate enhanced the performance of 2ASA by synergistic effects. The 2ASA molecules adsorbed on J55 steel spontaneously and exothermically by forming physisorbed monolayer. Tafel study shows that 2ASA behaved as mixed type inhibitor with domino inhibitive influence on anodic half reaction. Adsorption of 2ASA is facilitated by N, S, and O functionalities as checked by FTIR and EDS studies. The inhibitor blends so formulated could be used as alternative ecofriendly corrosion inhibitors for pickling and similar oilfield acidizing operations.

References

1. A. A. Olajire, *J. Mol. Liq.*, 248 (2017) 775.
2. A. Singh, Y. Lin, E. E. Ebenso, W. Liu, J. Pan, B. Huang, *J. Ind. Eng. Chem*., 24 (2015) 219.
3. E. B. Naveen, V. Ramnath, C. Elanchezhian, S. S. M. Nazirudeen, *J. Alloys Comp.*, 695 (2017) 3299.
4. X. Xu, A. Singh, Z. Sun, K. R. Ansari, Y. Lin, *R. Soc. Open Sci*., 4 (2017) 170933.
5. M. M. Askari, S. G. Aliofkhazraei, A. Hajizadeh, *J. Nat. Gas Science Eng.*, 58 (2018) 92.
6. P. Singh, A. Singh, M.A. Quraishi, *J. Taiwan Inst. Chem. Eng*., 60 (2016) 588.
7. Y. Lin, A. Singh, E. E. Ebenso, Y. Wu, C. Zhu, H. Zhu, *J. Taiwan Inst. Chem. Eng*., 46 (2015) 214.
8. A. Singh, K.R. Ansari, J. Haque, P. Dohare, H. Lgaz, R.S alghi, M.A. Quraishi, *J. Taiwan Inst. Chem. Eng*., 82 (2018) 233.
9. E. Ituen, O. Akaranta, A. James, S. Sun, *Sustain. Mater. Technol.*, 11 (2017) 12.
10. P. E. Alvarez, M. V. Fiori-Bimbi, A. Neske, S. A. Brandán, C. A. Gervasi, *J. Indus. Eng. Chem.*, 58 (2018) 92.
11. E. B. Ituen, O. Akaranta, S. A. Umoren, *J. Mol. Liq.*, 246 (2017) 112.
12. A. Singh, I. Ahamad, V. K. Singh, M. A. Quraishi, *J. Solid State Electrochem*., 15 (2011) 1087.
13. A. Singh, I. Ahamad, M. A. Quraishi, *Arab. J. Chem.*, 9 (2016) S1584.
14. Ambrish Singh, Y. Lin, W. Liu, S. Yu, J. Pan, C. Ren, D. Kuanhai, *J. Ind. Eng. Chem.*, 20 (2014) 4276.
15. E. B. Ituen, A. O. James, O. Akaranta, *Egypt. J. Pet.*, 26 (2017) 745.
16. A. Singh, K. R. Ansari, X. Xu, Z. Sun, A. Kumar, Y. Lin, *Sci. Report*., 7 (2017) 14904.
17. W. Xiaohong, P. Zhengwei, M. Lai, *Int. J. Electrochem. Sci*., 12 (2017) 11006.
18. A. Singh, Y. Lin, E. E. Ebenso, W. Liu, J. Pan, B. Huang, *J. Ind. Eng. Chem.,* 24 (2015) 219.
19. H. Feng, A. Singh, Y. Wu, Y. Lin, *New. J. Chem*., 42 (2018) 11404.
20. R. Wang, S. Luo, *Corros. Sci.*, 68 (2013) 119.
21. A. Singh, K. R. Ansari, A. Kumar, W. Liu, C. Songsong, Yuanhua Lin, *J. Alloys Comp*., 712 (2017) 121.
22. M. A. Quraishi, A. Singh, V. K. Singh, D. K. Yadav, A.K. Singh, *Mater. Chem Phys*. 122(2010) 114.
23. M. Finšgar, J. Jackson, *Corros. Sci.*, 86 (2014) 17.
24. E. B. Ituen, M. M. Solomon, S. A. Umoren, O. Akaranta, *J. Pet. Sci. Eng.*, 174 (2019) 984.
25. E. Ituen, V. kpenie, E. Ekemini. *Sci. Afri.* 3 (2019) e00075
26. H. Yang, M. Zhang, A. Singh, *Int. J. Electrochem. Sci*., 13 (2018) 9131.
27. Q. Zhang, S. Bolisttey, Y. Cao, s. Handschin, J. Adamcik, Q. Peng, R. Mezzenga. *Ange. Chemie.* 58 (2019) 6012.
28. H. Chen, S. Zhang, Z. Zhao, M. Liu, Q. Zhang. *J. Hazard. Mater.* 366 (2019) 669-676.
29. P. Shao, J. Tian, F. Yang, X. Duan, S. Gao, W. Shi, X. Luo, F. Cui, s. Luo, S. Wang. *Adv. Func. Mater.* 28 (2018) 1705295.
30. M. A. Bedair, M. M. B. El-Sabbah, A. S. Fouda, M. Elaryian, *Corros. Sci.*, 128 (2017) 45.
31. E. Ituen, O. Akaranta, A. James, *J. Bio Tribo Corros.*, 3 (2017) 23.
32. A. Singh, Y. Lin, I. B. Obot, E. E. Ebenso, K. R. Ansari, M. A. Quraishi, *Appl. Surf. Sci*., 356 (2015) 341.
33. X. Li, S. Tang, D. Yuan, J. Tang, C. Zang, N. Li, Y. Rao. *Ecotox. Environ. Safety.* 177 (2019) 77.
34. N. Li, S. Tang, Y. Rao, J. Qi, Q. Zhang, D. Yuan. Electrochim. Acta.298 (2019) 59.
35. A. Singh, Y. Lin, I. B. Obot. E. E. Ebenso, *J. Mol. Liq*., 219 (2016) 865.
36. K. Klodian, M. Finšgar, *New J. Chem.*, 41 (2017) 7151.

37. A. Singh, Y. Lin, K. R. Ansari, M. A. Quraishi, E. E. Ebenso, S. Chen, W. Liu, *Appl. Surf. Sci*., 359 (2015) 331.
38. L. Zhou, Y. L. Lv, Y. X. Hu, J. H. Zhao, X. Xia, X. Li, *J. Mol. Liq.*, 249 (2018) 179.
39. X. Wang, Z. Peng, S. Zhong, *Int. J. Electrochem. Sci*., 13 (2018) 8970.
40. A. Singh, K.R. Ansari, Y. Lin, M.A. Quraishi, H. Lgaz, I. M. Chung, *J. Taiwan Inst. Chem. Eng*., 95 (2019) 341.
41. A. Singh, M. Talha, X. Xu, Z. Sun, Y. Lin, *ACS Omega*, 2 (2017) 8177.
42. A. Singh, N. Soni, Y. Deyuan, A. Kumar, *Res. Phys*., 13 (2019) 102116.
43. P.T.C. Freire, F. E. A. Melo, J. M. Filho, *J. Raman Spect.*, 27 (1996) 507.
44. A. Singh, Y. Caihong, Y. Yaocheng, N. Soni, Y. Wu, Y. Lin, *ACS Omega*, 4 (2019) 3420.